Magnetocapacitive effects in the Néel *N*-type ferrimagnet $SmMnO_3$

Jong-Suck Jung,[1] Ayato Iyama,[1] Hiroyuki Nakamura,[1] Masaichiro Mizumaki,[2] Naomi Kawamura,[2] Yusuke Wakabayashi,[1] and Tsuyoshi Kimura[1]

[1]*Division of Materials Physics, Graduate School of Engineering Science, Osaka University, Toyonaka, Osaka 560-8531, Japan*

[2]*Japan Synchrotron Radiation Research Institute (JASRI/SPring-8), 1-1-1 Kouto, Sayo, Hyogo 679-5198, Japan*

(Received 9 October 2010; revised manuscript received 15 November 2010; published 13 December 2010)

Magnetocapacitive effects were investigated for Néel's *N*-type ferrimagnetic $SmMnO_3$, which shows temperature-induced magnetization reversal at the compensation temperature (T_{comp}=9.4 K) in a low magnetic field B ($<\sim 1$ T). When higher B is applied, remarkable anomalies were observed in the temperature profiles of magnetization, dielectric constant, and dielectric relaxation time around T_{comp}. These coupled field-induced anomalies give rise to striking magnetocapacitance and could be attributed to simultaneous reversals of ferrimagnetically coupled Sm and Mn moments. In addition, peculiar cooling-field dependent asymmetric magnetocapacitance was observed at T_{comp}.

DOI: 10.1103/PhysRevB.82.212403 PACS number(s): 75.85.+t, 75.60.−d, 77.22.Gm

Recent discoveries of spin-driven ferroelectricity and gigantic magnetoelectric effects in some multiferroics created considerable interest in terms of both basic and technological points of view.[1,2] Among such multiferroics, ferroelectricity in perovskite manganites, $RMnO_3$ (R=rare-earth ions), with the *Pbnm* orthorhombic structure originates from a spiral[3,4] or collinear E-type[5,6] antiferromagnetic (AFM) structure, breaking the inversion symmetry. These two magnetic structures are stabilized in $RMnO_3$ with intermediate (e.g., R =Tb and Dy) and small (e.g., R=Ho and Tm) ionic radii of the R ion r_R, respectively.[7,8] On the other hand, the ground state of $RMnO_3$ with large r_R (e.g., R=La, Sm, and Eu) is the paraelectric A-type AFM ordered phase in which Mn moments are aligned ferromagnetically within the *ab* plane but antiferromagnetically in the *c* direction.[9] More precisely, the A-type AFM structure possesses a canted component along the *c* axis. The origin of the canting has been discussed in terms of the single-ion anisotropy and the Dzyaloshinskii-Moriya interaction.[10] With or without the ferroelectricity, most of the above mentioned $RMnO_3$ show distinct dielectric dispersion at low temperatures only when an ac electric field is applied along the *c* axis.[7,11] The origin of the dielectric dispersion remains an open question.

In this study, we investigate the magnetocapacitive effects of $SmMnO_3$ possessing a relatively large r_R and the A-type AFM ground state of Mn moments. This manganite has never received attention mainly due to its lack of spin-driven ferroelectricity. However, $SmMnO_3$ shows distinct phenomena such as temperature-induced magnetization reversal and resultant negative magnetization opposite to the magnetic-field direction in a low magnetic field.[12] Such phenomena are observed in Néel's *N*-type ferrimagnetic compounds,[13] consisting of two or more magnetic sublattices (e.g., spinel ferrites[14]). In the case of $SmMnO_3$, the temperature-induced magnetization reversal and the negative magnetization are interpreted in connection with the canted Mn moments whose direction is the opposite of the polarized Sm moments.[12] Here, we report on dielectric anomalies coupled with the magnetization reversal induced by changes in temperature T and a magnetic field B for single crystals of $SmMnO_3$. We found that the dielectric properties are dominated by relative configurations of the polarized Sm and the canted Mn moments with respect to the direction of B.

Single crystals of $SmMnO_3$ were grown by the floating-zone method. The crystals were oriented by using Laue x-ray diffraction patterns and were cut into rectangular plates with the widest faces perpendicular to the *c* axis. The magnetization along the *c* axis (M_c) was measured with a commercial magnetometer. Real (ε_c') and imaginary (ε_c'') parts of the dielectric constant along the *c* axis were measured using an *LCR* meter with the frequency f range from 1 to 200 kHz. Magnetic fields were applied only along the *c* axis. To obtain the element-specific information in the net magnetization, we measured x-ray absorption (XAS) and x-ray magnetic circular dichroism (XMCD) spectra around Mn K and Sm $L_{2,3}$ edges for a powder sample crushed from a single crystal in transmission mode by using the helicity-modulation technique[15] on BL39XU at SPring-8.

Figures 1(a) and 1(b) show the T dependence of M_c and ε_c', respectively. Prior to every in-field measurement, magnetic fields were applied at 80 K [field cooling (FC)]. First, we focus on the data at zero (or very weak) magnetic fields. As shown in the data at 0.01 T of Fig. 1(a), a steep rise of M_c is observed at T_N=60 K, where the canted A-type AFM order of Mn moments arises. Upon cooling, M_c shows the maximum value of $\sim$0.1 μ_B/f.u. around 30 K and starts to decrease gradually below $\sim$30 K. As T decreases, it becomes zero at the compensation temperature T_{comp}=9.4 K and then becomes negative below T_{comp}. This T-induced magnetization reversal can be attributed to an antiparallel orientation between the canted Mn moment and the gradually polarized Sm moment induced by Sm-Mn exchange interactions.[12] Possible relative orientations between them above and below T_{comp} are schematically drawn in the insets of Fig. 1(a). Above T_{comp}, the vector sum of the canted Mn moments (M_{Mn}) is larger than the polarization of Sm moments (M_{Sm}). As T decreases, M_{Sm} grows rapidly and then exceeds M_{Mn} below T_{comp}, which causes the negative magnetization. This scenario is supported by the temperature profile of XMCD signals at 6.553 keV (Mn K edge) and 6.708 keV (Sm L_3 edge), represented by open triangles and squares in Fig. 1(a), respectively. The temperature profiles of the sum of the two XMCD signals [$=C\times$(Mn K)+(Sm L_3), where C

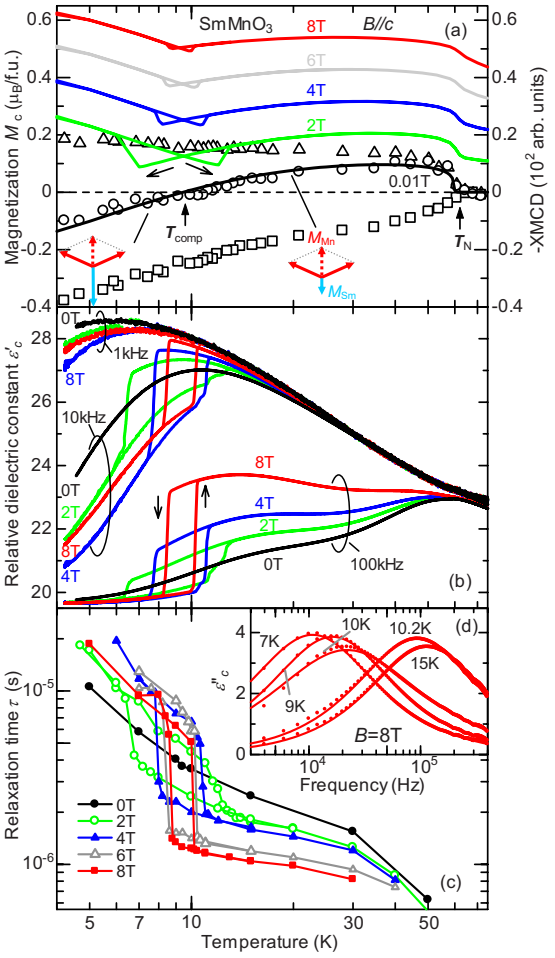

FIG. 1. (Color online) T profiles of (a) M_c, (b) ε_c', and (c) τ at selected B along c axis for single crystals of $SmMnO_3$. (d) f dependence of ε_c'' at $B=8$ T and selected temperatures. Solid lines are fits with the Cole-Cole function. Right axis of (a) open triangles and squares represent XMCD signals at 6.553 keV (Mn K edge) and 6.708 keV (Sm L_3 edge), respectively. Open circles represent the sum of these two XMCD signals [$=C\times$(Mn K)+(Sm L_3), where C is a constant value]. The inset of (a) depicts possible configurations of the polarized Sm and the canted Mn moments. Dashed arrows denote the vector sum of the canted Mn moments.

is constant] well overlaps with that of the low-field M_c-T curve [Compare open circles with black line in Fig. 1(a)].

As seen in Fig. 1(b), ε_c' strongly depends on f over a wide T range. Below $\sim T_N$, ε_c' is significantly suppressed with increasing f. At $B=0$ T, no clear anomaly was observed in the T dependence of ε_c' at around T_{comp}. The f profiles of ε_c' and ε_c'' are well fitted by the empirical Cole-Cole function, as reported for various RMnO$_3$.[11] From the fitting, we obtain the relaxation time τ which is given by $\tau=(2\pi f_p)^{-1}$, where f_p is the frequency of the ε_c'' peak. As shown in Fig. 1(c), τ gradually increases with decreasing T at $B=0$ T. Since the dielectric dispersion is evident below T_N, it is likely to be related to the magnetic ordering of the Mn moments.

Next, we focus on the data at $B\geq 2$ T. In contrast to the data at 0.01 T, the negative magnetization was not observed in M_c-T curves at $B\geq 2$ T [Fig. 1(a)]. Instead, M_c shows an abrupt increase at T_{jump} (just below T_{comp}) during the cooling

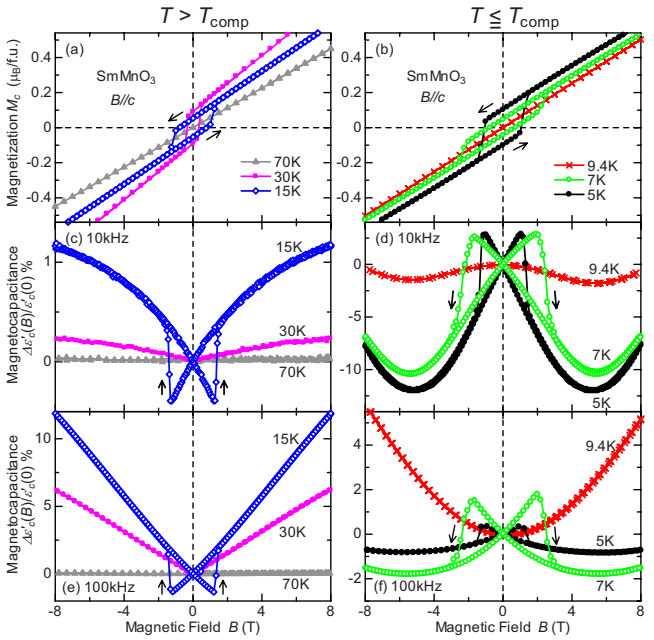

FIG. 2. (Color online) Isothermal magnetization curves measured at temperatures (a) above and (b) below T_{comp} for $SmMnO_3$. [(c)–(f)] Corresponding magnetocapacitance curves measured at 10 and 100 kHz. Magnetic fields are applied along the c axis.

process, and increases again as T decreases. The abrupt change at T_{jump} accompanies thermal hysteresis centered at T_{comp}, suggesting the existence of a first-order phase transition. These behaviors are detected at all B above 1 T but the hysteresis region gradually narrows down toward T_{comp} with increasing B.

Corresponding to the abrupt changes in M_c around T_{comp}, ε_c' measured in high B shows a sudden drop at T_{jump} with a thermal hysteresis. As seen in Fig. 1(b), the anomaly in ε_c' is not clear in the low-f (1 kHz) data but becomes pronounced with increasing f. The dielectric anomaly at T_{jump} is ascribed to the opposite magnetocapacitive effect, that is, the enhancement and the suppression of ε_c' by the application of B (up to ~ 6 T) above and below T_{jump}, respectively. In accordance with abrupt changes in M_c and ε_c', τ in high B data also show a sudden jump at T_{jump} [compare Fig. 1(c) with Figs. 1(a) and 1(b)]. For example, in the warming run at 8 T, an abrupt jump in M_c and ε_c' is observed at 10.1 K where $f_p=(2\pi\tau)^{-1}$ shows a rapid shift toward higher f, as seen in Fig. 1(d). These results show that the f-dependent magnetocapacitive effect in $SmMnO_3$ is ascribed to the change in τ by applying B.

To further examine the effects of B on M_c and ε_c, we measured the isothermal magnetization M_c and magnetocapacitance $\{\Delta\varepsilon_c'(B)/\varepsilon_c'(0)=[\varepsilon_c'(B)-\varepsilon_c'(0)]/\mathcal{E}(0)\}$ as functions of B. Figures 2(a) and 2(b) display M_c-B curves measured at selected temperatures above and below T_{comp}, respectively. At 70 K ($>T_N$), M_c is linearly dependent on B while hysteresis loops with sharp jumps at coercive magnetic fields B_{coer} due to magnetization reversal are observed at 30 and 15 K ($T_{comp}<T<T_N$). Below 30 K, the remanent magnetization M_{rem} decreases with decreasing T toward T_{comp} but the magnitude of B_{coer} increases. At $T_{comp}=9.4$ K, the hysteresis be-

havior becomes negligible and M_c shows a linear B dependence again. With further decreasing T, hysteresis loops appear again, and $M_{\rm rem}$ ($B_{\rm coer}$) increases (decreases) toward lower T, as seen in the 7 K and the 5 K data of Fig. 2(b).

Isothermal magnetocapacitance measurements were done at ac electric fields of 10 kHz [Figs. 2(c) and 2(d)] or 100 kHz [Figs. 2(e) and 2(f)], at which the most pronounced magnetocapacitive effects were observed. At 70 K ($>T_{\rm N}$), magnetocapacitance is negligibly small while it becomes evident at $T_{\rm comp}<T<T_{\rm N}$. As seen in Figs. 2(c) and 2(e), the magnitude of $\Delta\varepsilon_c'(B)/\varepsilon_c'(0)$ increases with decreasing T, and a clear butterfly shape is observed in the $\Delta\varepsilon_c'(B)/\varepsilon_c'(0)$-$B$ curve at 15 K. At $T_{\rm comp}$=9.4 K, the hysteresis in $\Delta\varepsilon_c'(B)/\varepsilon_c'(0)$ disappears again [Figs. 2(d) and 2(f)], which also corresponds to the disappearance of the hysteresis in M_c. Below $T_{\rm comp}$, the butterfly-shaped magnetocapacitance shows up again in accordance with the re-emergence of the hysteresis behavior in M_c. The observed butterfly curves can be ascribed to the magnetization reversal process because the magnetic field where $\Delta\varepsilon_c'(B)/\varepsilon_c'(0)$ increases abruptly corresponds well to $B_{\rm coer}$ in each M_c-B curve. The magnetocapacitance curves above and below $T_{\rm comp}$ show a sharp contrast, though both of them exhibit the butterfly-shaped hysteresis, and the corresponding M_c-B curves show similar hysteresis loops. Above $T_{\rm comp}$, $\Delta\varepsilon_c'(B)/\varepsilon_c'(0)$ abruptly increases at $B_{\rm coer}$ [Figs. 2(c) and 2(e)] whereas it shows a sudden drop below $T_{\rm comp}$ [Figs. 2(d) and 2(f)]. In other words, the features of the magnetocapacitance above and below $T_{\rm comp}$ are opposite in sign to each other.

Figure 3(a) displays the B-T phase diagram in which phase boundaries were determined by $T_{\rm jump}$ [circles] or $B_{\rm coer}$ [triangles]. The phase diagram clearly shows that the $T_{\rm jump}$ at which the anomalies were observed in the M_c-T and ε_c'-T curves overlaps $B_{\rm coer}$ at which the magnetization reversal occurs. The gray area in the phase diagram represents the hysteresis region. With increasing B at around $T_{\rm comp}$, $B_{\rm coer}$ shows a tendency to diverge and $T_{\rm jump}$ approaches $T_{\rm comp}$ from both the low- and the high-T ends. Such a tendency is often observed in Néel's N-type ferrimagnetic compounds.[16] We schematically illustrate possible orientations of $M_{\rm Sm}$ and $M_{\rm Mn}$ with respect to $B\|c$ in each phase [insets of Fig. 3(a)]. At $|B|\leq\sim 0.5$ T, the system cannot cross the phase boundary down to the lowest T. Therefore, there is no change in the relative configurations of $M_{\rm Sm}$ and $M_{\rm Mn}$ with respect to B, and the negative magnetization state appears. By contrast, at $|B|>\sim 0.5$ T, the system does cross the boundary at $T_{\rm jump}$. When the energy of applied B exceeds the magnetic anisotropy energy, the states with positive magnetization may become more stable. Thus, the reversals of both $M_{\rm Sm}$ and $M_{\rm Mn}$ [right insets$\leftrightarrow$left insets of Fig. 3(a)] are likely to occur at $T_{\rm jump}$.

The reversals of $M_{\rm Sm}$ and $M_{\rm Mn}$ in crossing the phase boundary were demonstrated by XMCD measurements. Figures 3(b)–3(d) show the XAS (upper) and the XMCD (lower) spectra around Mn K, Sm L_3, and Sm L_2 edges, respectively. For these measurements, the sample was first field cooled down to 2 K at 0.5 T. Subsequently, the spectra were taken at 0.5 T ($<B_{\rm coer}$) and then at 4 T ($>B_{\rm coer}$). In all three spectra, the XMCD signals at 4 T are opposite in sign to those at 0.5 T. This result indicates that both $M_{\rm Sm}$ and $M_{\rm Mn}$

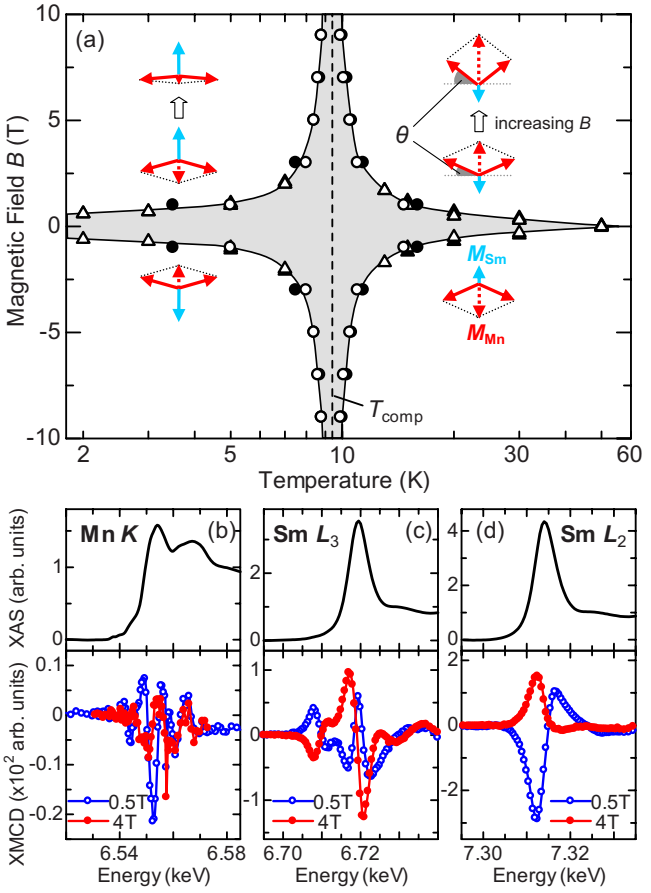

FIG. 3. (Color online) (a) Magnetic phase diagram of $SmMnO_3$. Illustrations in the inset depict possible configurations of polarized Sm [light blue (gray) arrows] and canted Mn [red (black) arrows] moments in the respective phases. Open and closed triangles represent $B_{\rm coer}$ obtained from the M_c-B and the ε_c'-B curves, respectively. Open and closed circles represent $T_{\rm jump}$ obtained from the M_c-T and the ε_c'-T curves, respectively. The gray area represents the hysteresis region. (b), (c), and (d) show XAS and XMCD signals of Mn K, Sm L_3, and Sm L_2 edges, respectively, at 2 K. After field cooling at 0.5 T, the measurements were done at 0.5 and 4 T.

are reversed when crossing the phase boundary, as illustrated in the insets of Fig. 3(a).

Let us discuss the origin of the distinctive magnetocapacitive effect in $SmMnO_3$. Since $M_{\rm Mn}$ is expected to be parallel to B above $T_{\rm jump}$, the canting angle of the Mn moments (θ) becomes large with increasing B [upper-right inset of Fig. 3(a)]. By contrast, θ becomes small with increasing B below $T_{\rm jump}$ where $M_{\rm Mn}$ is antiparallel to B [upper-left inset of Fig. 3(a)]. Thus, the application of B yields opposite effects on θ above and below $T_{\rm jump}$. As seen in Fig. 1(c), τ decreases monotonically with increasing B above $T_{\rm jump}$ while τ increases with increasing B up to $\sim$5 T below $T_{\rm jump}$. The change in τ by applying B well corresponds to that in θ, which suggests that the change in θ plays an important role in the observed magnetocapacitive effect characterized by τ. Furthermore, sudden changes in τ as well as ε_c' at $T_{\rm jump}$ (or $B_{\rm coer}$) can be also explained in terms of an abrupt change in θ. When the system crosses a boundary between phases with $M_{\rm Mn}$ parallel and antiparallel to B at $T_{\rm jump}$ (or $B_{\rm coer}$), θ should

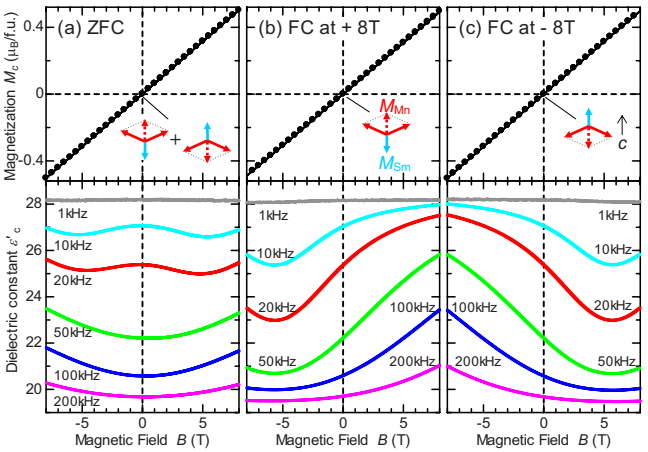

FIG. 4. (Color online) B dependence of M_c and ε'_c at T_{comp} =9.4 K after (a) ZFC, (b) FC at +8 T, and (c) FC at B=−8 T procedures. The insets show possible configurations of M_{Mn} and M_{Sm} in the respective cooled states.

also change abruptly. Although the microscopic mechanism of the close correlation between θ on τ is still unclear, the present finding will provide a clue to understanding the dielectric dispersion observed in RMnO$_3$.[7,11]

Finally, we present the peculiar cooling-field dependent asymmetric magnetocapacitance observed at T_{comp}. Figure 4 shows the B profiles of M_c and ε'_c at 9.4 K (=T_{comp}). The data in Figs. 4(a)–4(c) were measured after the zero FC (ZFC), the FC at +8 T, and the FC at −8 T, respectively. Regardless of the cooling procedures, all the M_c-B curves show exactly the same B-linear behavior and pass through the origin (upper panels of Fig. 4), which means that the system behaves as an antiferromagnet at T_{comp}. By contrast, the ε'_c-B curves strongly depend on the cooling process. In the ZFC data, the ε'_c-B curves display symmetric appearances centering around B=0 T while the ε'_c-B curves after the FC at +8 and −8 T are asymmetric and show mirror-reversed appearances of each other. The observed cooling-process dependence on the magnetocapacitance can be explained by considering the existence of two types of domains whose volume ratio depends on the cooling procedure, as illustrated in the insets of Fig. 4.

In summary, we investigated the magnetocapacitive effects of Néel's N-type ferrimagnetic SmMnO$_3$ showing temperature-induced magnetization reversal due to keen competition between ferrimagnetically coupled polarized Sm and canted Mn moments. We found first-orderlike anomalies in the magnetic and dielectric properties around the compensation point, which consequently causes the large magnetocapacitive effects. The simultaneous reversals of the coupled Sm-Mn moments induced by applied magnetic fields are ascribed to the anomalies. Furthermore, we observed the peculiar asymmetric magnetocapacitance at the compensation temperature.

We thank T. Nakano for fruitful discussions. This work was supported by KAKENHI (Grants No. 20674005 and No. 20001004) and the Global COE Program (G18) of the JSPS. The XAS-XMCD measurements at BL39XU (Proposal No. 2010A1133) in SPring-8 were performed with the approval of the JASRI.

[1] T. Kimura, T. Goto, H. Shintani, K. Ishizaka, T. Arima, and Y. Tokura, Nature (London) **426**, 55 (2003).
[2] S.-W. Cheong and M. Mostovoy, Nature Mater. **6**, 13 (2007).
[3] M. Kenzelmann, A. B. Harris, S. Jonas, C. Broholm, J. Schefer, S. B. Kim, C. L. Zhang, S.-W. Cheong, O. P. Vajk, and J. W. Lynn, Phys. Rev. Lett. **95**, 087206 (2005).
[4] M. Mostovoy, Phys. Rev. Lett. **96**, 067601 (2006).
[5] I. A. Sergienko, C. Sen, and E. Dagotto, Phys. Rev. Lett. **97**, 227204 (2006).
[6] V. Yu. Pomjakushin, M. Kenzelmann, A. Dönni, A. B. Harris, T. Nakajima, S. Mitsuda, M. Tachibana, L. Keller, J. Mesot, H. Kitazawa, and E. Takayama-Muromachi, N. J. Phys. **11**, 043019 (2009).
[7] T. Goto, T. Kimura, G. Lawes, A. P. Ramirez, and Y. Tokura, Phys. Rev. Lett. **92**, 257201 (2004).
[8] S. Ishiwata, Y. Kaneko, Y. Tokunaga, Y. Taguchi, T. H. Arima, and Y. Tokura, Phys. Rev. B **81**, 100411(R) (2010).
[9] T. Kimura, S. Ishihara, H. Shintani, T. Arima, K. T. Takahashi, K. Ishizaka, and Y. Tokura, Phys. Rev. B **68**, 060403(R) (2003).
[10] V. Skumryev, F. Ott, J. M. D. Coey, A. Anane, J.-P. Renard, L. Pinsard-Gaudart, and A. Revcolevschi, Eur. Phys. J. B **11**, 401 (1999).
[11] F. Schrettle, P. Lunkenheimer, J. Hemberger, V. Yu. Ivanov, A. A. Mukhin, A. M. Balbashov, and A. Loidl, Phys. Rev. Lett. **102**, 207208 (2009).
[12] V. Yu. Ivanov, A. A. Mukhin, A. S. Prokhorov, and A. M. Balbashov, Phys. Status Solidi B **236**, 445 (2003).
[13] L. Néel, Ann. Phys. (Paris) **3**, 137 (1948).
[14] N. Menyuk, K. Dwight, and D. G. Wickhan, Phys. Rev. Lett. **4**, 119 (1960).
[15] M. Suzuki, N. Kawamura, M. Mizumaki, A. Urata, H. Maruyama, S. Goto, and T. Ishikawa, Jpn. J. Appl. Phys., Part 2 **37**, L1488 (1998).
[16] For example, J. P. Hanton and A. H. Morrish, J. Appl. Phys. **36**, 1007 (1965).